ICAS 2021 SHANGHAI
International Council of the Aeronautical Sciences
32nd Congress of the International Council of the Aeronautical Sciences
September 6-10, 2021
Pudong Shangri-La, Shanghai, China

BAYESIAN APPROACH TO SIMULTANEOUS STATIC AND DYNAMIC FLIGHT CHARACTERISTICS MODELING

Masaru Naruoka[1]

[1]Japan Aerospace Exploration Agency (JAXA)

Abstract

A Modeling method of flight characteristics of an aircraft by using flight data was discussed in this study. As an example, lift and drag aerodynamic force worked on a fixed-wing aircraft was studied. In order to get its accurate and reliable model, a statistical approach with Markov chain Monte Carlo sampling technique based on Bayesian inference, which estimates not only target parameters but also their distribution, was utilized. Additionally, a newly postulated model taking both static and dynamic components into account was applied. It could deal with approximately ten times more and untidy flight data compared to the author's previous study. The estimated results were successfully approximated the data acquired with actual flights. In addition, by showing the deterioration of the estimation without the consideration of the dynamic components due to the mismatch between the data and model, the effectiveness of the proposed method was demonstrated.

Keywords: Bayesian estimation, Markov chain Monte Carlo, Flight characteristics

1. Introduction

To estimate flight characteristics of an aircraft by using observed flight data is performed for various purposes. Firstly, it is performed as one of the important tasks in the development phase of an aircraft. Aircraft stability and controllability are estimated and validated with flight test data, which is required by regulation for airworthiness. In addition, from the point of view to develop a competitive aircraft, to estimate its characteristics as accurately as possible is essential, because it enables to make its performance to be guaranteed more attractive.

The estimation results are also useful for aircraft operation. An operator of an aircraft can maintain the performance of an aircraft effectively by using the estimation results. For example, monitoring the drag will optimize the interval period of cleaning an aircraft. Moreover, this estimation will contribute enhancement of the traffic capacity of airspace. The capacity enhancement is typically planned by using simulations, which require an accurate mathematical model of flight characteristics. In addition to typical models represented by the Base of Aircraft Data (BADA) [1], which are built based on proprietary knowledge of an airframer, to obtain a more accurate model by using the estimation technique with flight data has been actively studied recently [2].

As mentioned above, there is various utilization of the estimation of the flight characteristics, and their common requirements are accuracy and reliability of the estimated results. Thus, the author has been focused on a Bayesian approach to this estimation problem, because the approach has preferable two features: It provides not only point estimation results but also a distribution of the results, which can be used as metrics for how reliable the results are. In addition, the estimation results can be controllable based on prior knowledge. Compared to parameter estimation methods typically applied to the flight characteristics estimation represented by least square and Kalman filtering described in text books [3, 4], these advantages are still maintained. The typical methods can provide covariances of estimated results, however, the covariances are just parts of distribution information of the results. Additionally, it is relatively difficult to regulate the estimation results of these methods based on prior knowledge, because indirect ways such as the application of weights or extended state values are required.

By utilizing those features of the Bayesian approach, the author previously studied the estimation of static components of lift and drag aerodynamic coefficients of an airplane [5]. The previous study was intended to obtain the estimated results in enough reliability to compare with results of wind tunnel tests or computational fluid dynamics (CFD) analyses. The results obtained with flight data of a Cessna 680 Citation Sovereign, shortly C680, owned by JAXA were reasonable. The previous study was concluded that the estimation with Markov chain Monte Carlo (MCMC) well summarized in Chapter.11 of Bishop [6], which is a random sampling technique to get parameter distribution based on Bayesian inference, was basically effective for the static flight characteristic modeling.
The goal of this study is identical to the previous study, and the author has been motivated to improve the reliability of the estimation by using more flight data. However, a straightforward application of the previous method to the large dataset was insufficient. Consequently, dynamic components are additionally taken into consideration in this study. The dynamic components are estimated with the static ones simultaneously. There is another way to treat the dynamic component separately, which may succeed practically by using parts of flight having much clue for the estimation of the dynamic component represented by maneuvering. However, actual flight always experiences more or less effect derived from both components. Therefore, the simultaneous estimation is oriented in this study.
In the following, the details of the estimated targets and methods are explained. In section 2, the lift and drag components to be estimated are clarified with equations. Flight data used as the inputs for the estimation are also described. In addition, Stan [7], a MCMC sampling software, and its application to this study are elaborated. Then, the estimation results are explained in section 3. Three cases of estimation results are compared: the large dataset with and without the consideration of the dynamics components, and the same small dataset as the previous study without the consideration. The failure of the estimation by using the large dataset without the consideration of the dynamics components is especially discussed according to the lift estimation results. Finally, this study is concluded in section 4.

2. Estimation preparation

This section summarizes the preliminary steps in the estimation. First, lift and drag aerodynamic parameters of a fixed-wing aircraft are factorized into elements, where the parameters to be estimated and inputs are clarified. Then, the flight data of C680 used as the inputs are explained. Finally, the application of Stan, the utilized MCMC sampler, is described.

2.1 Lift and drag models

The lift and drag models are postulated based on the knowledge described in Jategaonkar [3], Raymer [8], and Filippone [9]. The lift coefficient C_L is factorized in a linearized form as

$$C_L \approx \underbrace{C_{L0} + C_{L\alpha}\,\alpha + C_{L\delta_e}\,\delta_e}_{\text{static components}} + \underbrace{C_{L\dot{\alpha}}\,q}_{\text{dynamic component}} \quad , \tag{1}$$

where α, δ_e, and q are angle of attack, elevator deflection angle, and pitch angular speed, respectively. The symbol C_Ls with subscripts on the right side are the parameters to be estimated, and as well-known, C_{L0} and $C_{L\alpha}$ are the zero lift coefficient and lift slope, respectively. The other symbols including C_L on the left side are the inputs for the estimation. The significant point of this model is the inclusion of the last term on the right side. It is the dynamic component of the lift while the other terms are the static components, which have been taken into the account in the previous study. It is noted that the pitch angular speed q are used for its inputs instead of the time derivative of the angle of attack $\dot{\alpha}$ although its coefficient is represented as $C_{L\dot{\alpha}}$. This is because q is directly measured with an inertial measurement unit (IMU), and is assumed to be more accurate than $\dot{\alpha}$. On the other hand, $\dot{\alpha}$ is only acquired by taking time difference of α.
Although there are other aerodynamic devices to be considered, they are intentionally dropped from the model as same as the previous study. It is known that if there is a strong correlation between two inputs the estimation may deteriorate. According to this knowledge, a term of the stabilizer, whose deflection angle δ_{stb} has strong linearity to the angle of attach α shown in section 2.2, is dropped. In

addition, other aerodynamic devices represented by flaps, spoilers, and gears are not included in the model for simplicity. In order to eliminate their contribution, the flight data obtained in the non-clean configurations are intentionally excluded from the inputs, which will be also indicated in section 2.2. The drag coefficient C_D is modeled as

$$C_D \approx \underbrace{C_{D0} + 20\left(\max\left(M - M_0, 0\right)\right)^4}_{\text{static components}} + \underbrace{C_{Di}{C_L}^2}_{\text{both components}} , \tag{2}$$

where being similar to Eq. (1), the symbol C_Ds with subscripts in the right side are the estimation targets. The first and second terms on the right side represent the parasite drags while the third term corresponds to the induced drag. The wave drag, which is one of the parasite drags and resulted from the formation of shocks, is specially treated with the second term, which is configured to be effective when the Mach number M exceeds a base Mach number M_0 to be estimated. This representation is the same as an equation described in Filippone [9] as

$$C_{D\text{wave}} = 20\left(M - M_c\right)^4, \quad M > M_c\,, \tag{3}$$

where M_c is the critical Mach number. The last term is linear to square of the lift coefficient ${C_L}^2$, and represents the induced drag, which includes both static and dynamic components. The reason why the effects of other aerodynamic devices are not taken into account is the same as that of the lift modeling. C_D, C_L, and M are the inputs given by the flight data.
In section 3.2, there is a comparison of the models with and without the consideration of the dynamic components. The model with the consideration corresponds to Eqs. (1) and (2). On the other hand, the without model uses the same Eq. (2), but

$$C_L \approx C_{L0} + C_{L\alpha}\,\alpha + C_{L\delta_e}\,\delta_e \tag{4}$$

instead of Eq. (1).

2.2 Input flight data

The flight data used for this study is the same as the previous study except for the number of samples to be used for the estimation inputs. The data acquisition and preprocessing methods are explained. The original flight data is obtained by the C680 named as “Hisho” shown in Fig. 1, which is modified by Japan Aerospace Exploration Agency (JAXA) to be used for various flight experiments [10]. A C680 is a fixed-wing aircraft with twin turbojet engines. Thanks to the modification, the acquired data is composed of as many types of data as available. For instance, the motion information represented by acceleration and angular speed, deflection angles of aerodynamic devices, and engine data through interface complied to full authority digital engine controller (FADEC) are available. The angle of attack and airspeed are accurately measured with sensors mounted in front of its nose boom. Its thrust and weight in flight estimated with dedicated software in certain accuracy are included in the data.

Figure 1 – Research aircraft “Hisho”, which means fly higher in Japanese

Figure 2 shows the preprocessing of the flight data of the previous and current studies. The flight data is preprocessed to filter out the non-clean configuration parts, in which the flaps, spoilers, or gears

of the aircraft are activated. Additionally, the data obtained at an altitude below 15,000 ft, where the aircraft may not be almost in the clean configuration due to taking off or landing operations, is excluded. Furthermore, turning flights are dropped from the data because the estimated targets are limited to the longitudinal characteristics this time; the threshold roll angles are $\pm 2^{\circ}$. In the previous study, the further selection was performed in order to extract data in trimmed conditions where acceleration or rotation is negligibly small. Such selection is not applied in this study, and 9040 samples of approximately ten times of 732 samples of the previous study are used for the estimation, which are called the large and small datasets, respectively.

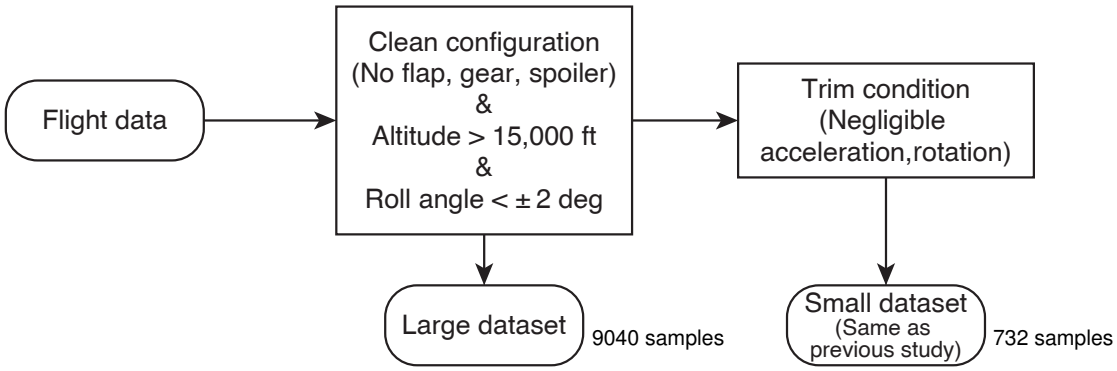

Figure 2 – Flight data preprocessing

Figure 3 shows the trajectory recorded in the flight data. The red lines, which correspond to 18.7 hours long of 10 flights, are used as the inputs. The total flights shown in the thin grey lines without the preprocessing are 43.8 hours long. The used flight data sufficiently covers the envelope of the aircraft illustrated by the dot lines, whose ceiling altitude and maximum Mach number are 47,000 ft and 0.80.

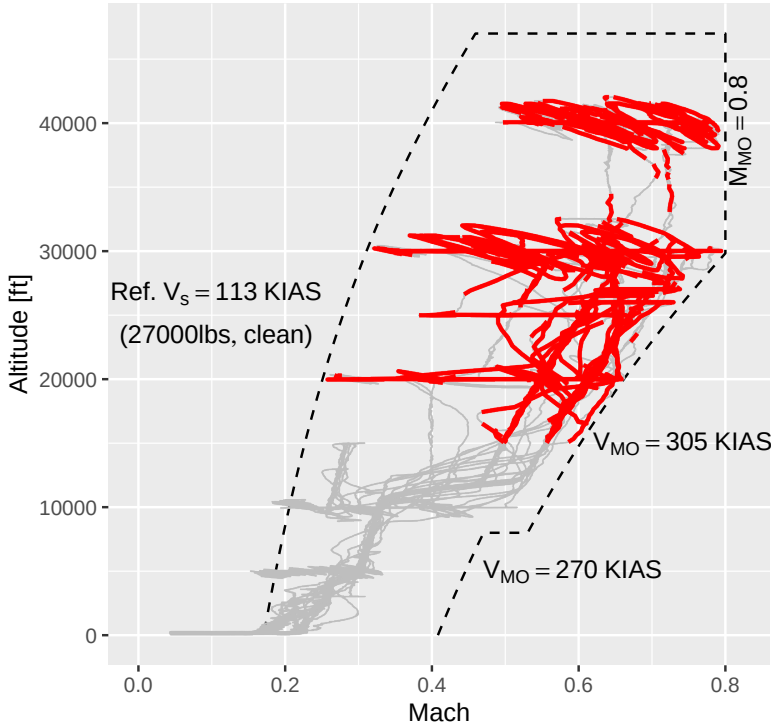

Figure 3 – Trajectory recorded in flight data

The coefficients of lift C_L and drag C_D described in Eqs. (1)-(2) are the inputs for the estimation, which calculated with the flight data as

$$\begin{bmatrix} C_L \\ C_D \end{bmatrix} = \frac{1}{qS} \left[\mathrm{Rot}(\alpha, \beta) \left(m\vec{a} - \vec{T} \right) \right]_{z,x}, \tag{5}$$

where q, S, m, $\vec{a}$, and $\vec{T}$ are dynamic pressure, wing area, weight, outputs of an accelerometer strapped down to the body, and thrust, respectively. $\mathrm{Rot}(\alpha,\beta)$ is a rotation matrix composed of angle of attack α and side slip angle β. $[\cdot]_{z,x}$ represents taking upward and forward elements from a three dimensional vector.

Figures 4 summarizes the input flight data used for the lift and drag estimations corresponding to Eqs. (1) and (2). Each figure consists of three parts: the diagonal, lower and upper triangle elements correspond to the histogram of each input, scatter, and correlation plots of each pair of two inputs, respectively. The correlation plots are annotated with scaled Spearman's rank correlation coefficients, whose -100 and 100 represent fully positive and negative correlations. As shown in Fig. 4a, the angle of attack α and stabilizer deflection δ_{stab} are strongly correlated by -97 of the coefficient, that is the reason the stabilizer term was dropped from Eqs. (1) and (2). It is noted that although Reynold's number Re is not included in the postulated model, it is displayed in Fig. 4b just for reference.

2.3 Utilization of Stan

Although the general explanation of Bayesian estimation and MCMC sampling is omitted due to the page limitation, detailed information about the application of Stan, the MCMC sampled utilized in this study, is provided. Stan generates samples of parameters to be estimated based on observation, that is, input flight data. The samples are internally adjusted with a postulated statistical model used for the likelihood calculations. The model should be provided by a user in a specific format in addition to the flight data.

Listing 1 shows the script to transfer the model to Stan. Basically, it is configured according to Eqs. (1) and (2) as shown in its "model" section. C_L and C_D are assumed to be normally distributed with their standard deviations of $\sigma(C_L)$ and $\sigma(C_D)$, respectively. The "data" section defines the structure of the input flight data. The section named "parameters" lists the main parameters to be estimated. It should be stressed that special constrains are provided to C_{Di} and M_0. C_{Di} is the coefficient of the induced drag:

$$C_{Di} \equiv \frac{1}{e\pi \mathcal{A}\mathcal{R}}, \tag{6}$$

where e is the Oswald efficiency known to be one at maximum. $\mathcal{A}\mathcal{R}$ is the aspect ratio of the main wing by 7.731 for C680. M_0 is the base Mach number to represent the effect of the wave drag, which is typically significant in transonic. Thus, M_0 is bonded to be greater than 0.55 with margin. $\sigma(C_L)$ and $\sigma(C_D)$ are also bounded to be greater than zero because of standard deviations. The following "transformed parameters" helps "parameter" section to define the auxiliary parameters. It is noted that the above mention corresponds to the model with the dynamic components. For the model without the dynamic components, the 30th line in Listing 1 is commented out.

For each estimation with Stan, 2000 iterations are performed to draw the parameter samples from four independent generators (chains). The first 1000 iterations are used as "burnin", that is, the startup phase to wait for the parameter distribution being converged, and are not included in the post analyses. In addition, every two of three iteration results are excluded from the final samples in order to mitigate autocorrelation. To summarize the numbers, 1336 samples $(= (2000-1000)\times 4/3)$ of each estimated parameter are generated par one estimation trial. The convergence of the distribution of the generated samples is evaluated with the $\hat{R}$ index in addition to a visual check of the histories of the iterations as shown in the next section.

3. Estimation results

In the following, the best estimation results obtained with the large dataset and inclusion of the dynamic components are shown. Then, its effectiveness is discussed via the comparison of the lift estimation results obtained with the three combinations of the datasets and models. Additionally, the estimation of the wave drag is discussed.

3.1 Best estimation results

The best estimation was performed by using the large dataset with the dynamic component consideration. Its results are shown in Table 1, which summarizes the statistical values of the estimated parameters. Figure 5 shows their histograms. It is noted that although the baseline coefficients of the

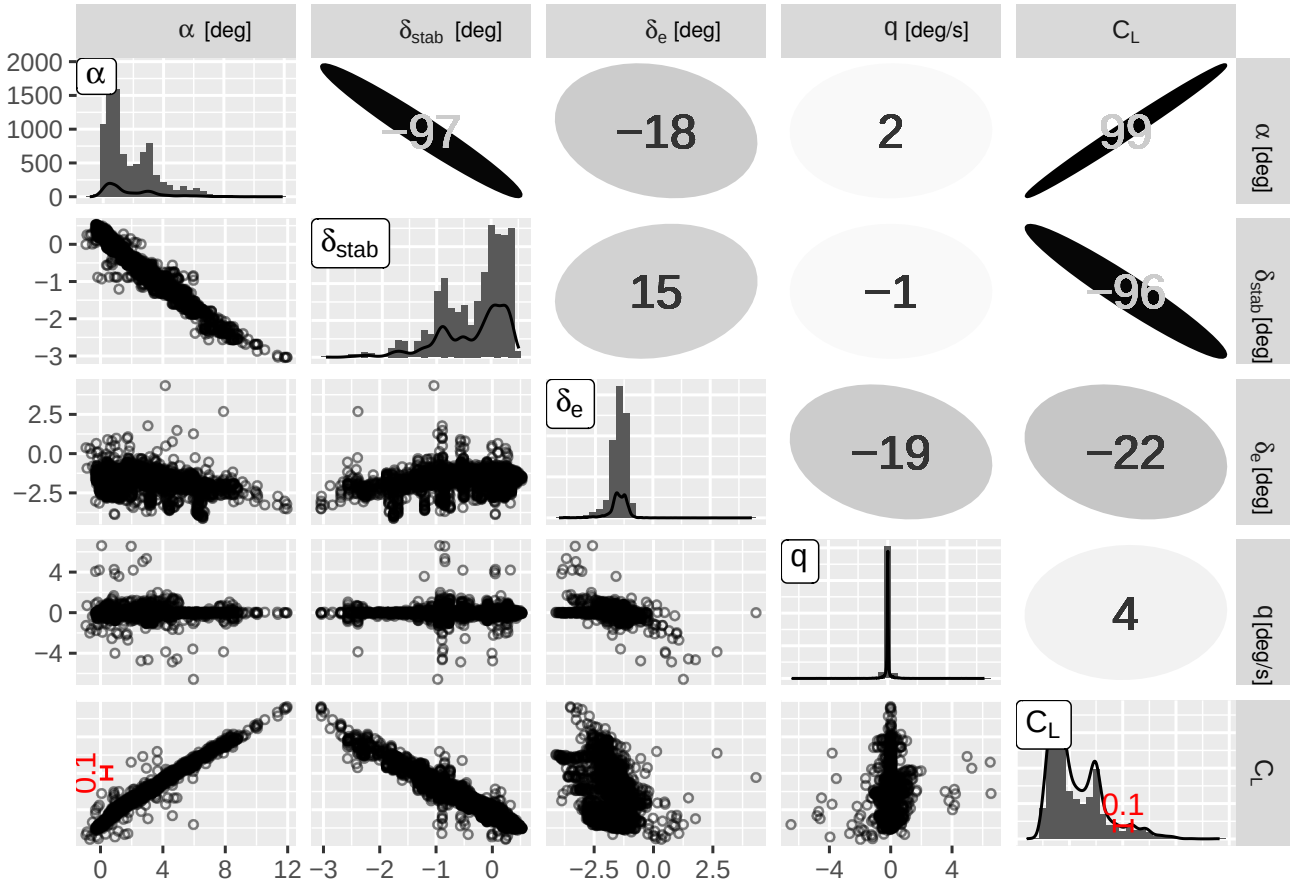

(a) For C_L estimation

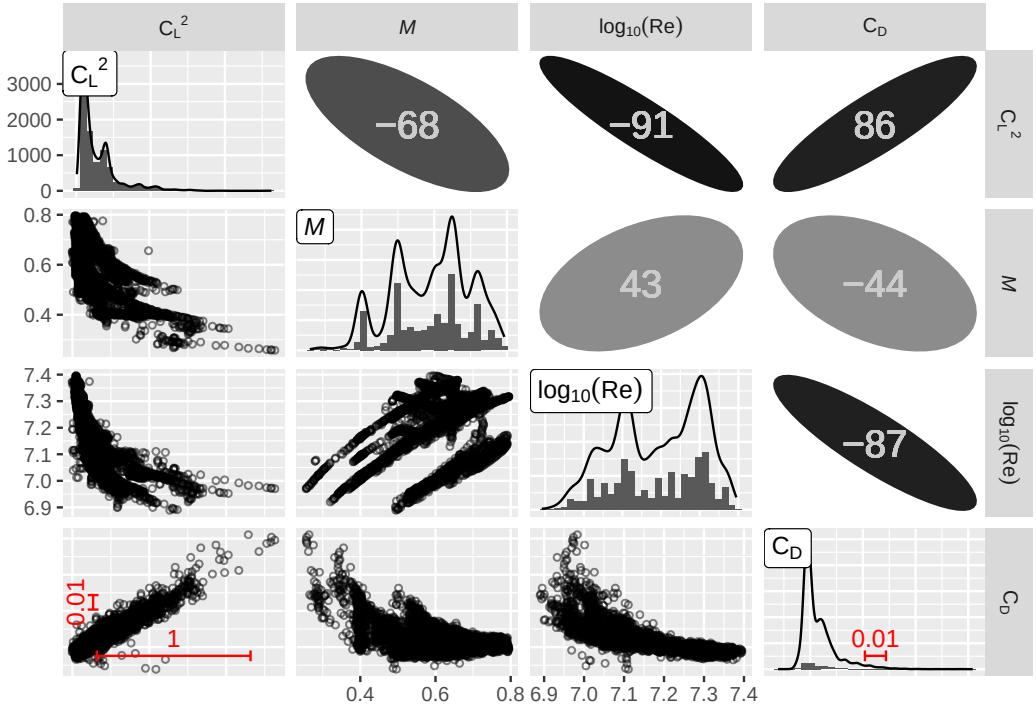

(b) For C_D estimation. Reynold's number Re is for reference.

Figure 4 – Pair plots of input flight data. The symbols are same as those in Eq. (1) and (2). For each set, the diagonal elements show histograms. The elements in the lower and upper triangle areas are scatter and correlation plots of each two variables, respectively.

Listing 1: Model for Stan

```
data {
  int<lower=1> N; // Number of samples
  vector[N] alpha_deg; // α
  vector[N] de_deg; // δ_e
  vector[N] q_dps; // q
  vector[N] cL; // C_L
  vector[N] mach; // M
  vector[N] cD; // C_D
}
parameters {
  real cL0; // C_L0
  real cLa; // C_Lα
  real cLde; // C_Lδe
  real cLadot; // C_Lq
  real<lower=0> sigma_cL; // σ(C_L)
  real cD0; // C_D0
  real<lower=1.0/(pi()*7.731)> inv_epar; // C_Di
  real<lower=0.55, upper=0.9> mach0; // M_0
  real<lower=0> sigma_cD; // σ(C_D)
}
transformed parameters {
  vector[N] mach_delta_tmp;
  for(i in 1:N){
    mach_delta_tmp[i] = (mach[i] >= mach0) ? pow(mach[i] - mach0, 4) : 0;
  }
}
model {
  cL ~ normal(
      cL0 + (cLa * alpha_deg) + (cLde * de_deg)
        + (cLadot * q_dps),
      sigma_cL); // Eq. (1)
  cD ~ normal(
      cD0 + (inv_epar * (cL .* cL)) + (20 * mach_delta_tmp),
      sigma_cD); // Eq. (2)
}
```

lift C_{L0} and drag C_{D0} were estimated, their relative differences from their mean values are displayed as ΔC_{L0} and ΔC_{D0}, respectively.

The first step to evaluate the estimation results acquired with the MCMC sampler is to check the convergence of the distribution of the generated samples. This convergence is partially proved for the goodness of the model postulation and the successfulness of the estimation. The evaluation of the convergence is quickly performed by the $\hat{R}$ indices in Table 1. According to Chapter 11 of Gelman [11], $\hat{R} < 1.1$ means that the distribution of the corresponding parameter has been sufficiently converged. As shown in the table, all $\hat{R}$ satisfied this condition. In addition, the convergence was visually checked with the trace plots of the samples in Fig. 6. The plots show that the samples are not biased between the chains and are randomly moved, thus, the convergence successfully occurred.

Table 1 – Summary of estimated parameters

Item	Mean	Standard deviation	2.5%	Median (50%)	97.5%	$\hat{R}$
ΔC_{L0}	(0.000)	7.187×10^{-4}	-1.383×10^{-3}	1.260×10^{-5}	1.438×10^{-3}	9.986×10^{-1}
$C_{L\alpha}$ [*1]	8.594×10^{-2}	1.166×10^{-4}	8.571×10^{-2}	8.594×10^{-2}	8.616×10^{-2}	9.981×10^{-1}
$C_{L\delta_e}$	-1.663×10^{-3}	5.070×10^{-4}	-2.665×10^{-3}	-1.644×10^{-3}	-6.465×10^{-4}	9.986×10^{-1}
$C_{L\dot{\alpha}}$ [*2]	3.768×10^{-2}	6.932×10^{-4}	3.635×10^{-2}	3.770×10^{-2}	3.911×10^{-2}	9.989×10^{-1}
$\sigma(C_L)$	1.798×10^{-2}	1.292×10^{-4}	1.774×10^{-2}	1.798×10^{-2}	1.822×10^{-2}	1.001
ΔC_{D0}	(0.000)	4.620×10^{-5}	-8.708×10^{-5}	-1.200×10^{-6}	8.954×10^{-5}	1.001
M_0	6.624×10^{-1}	1.346×10^{-3}	6.599×10^{-1}	6.623×10^{-1}	6.650×10^{-1}	1.006
C_{Di}	5.934×10^{-2}	2.303×10^{-4}	5.889×10^{-2}	5.934×10^{-2}	5.981×10^{-2}	1.001
$\sigma(C_D)$	2.873×10^{-3}	2.107×10^{-5}	2.831×10^{-3}	2.872×10^{-3}	2.916×10^{-3}	1.001

[*1] $[1/\mathrm{deg}]$ [*2] $[1/(\mathrm{deg/s})]$

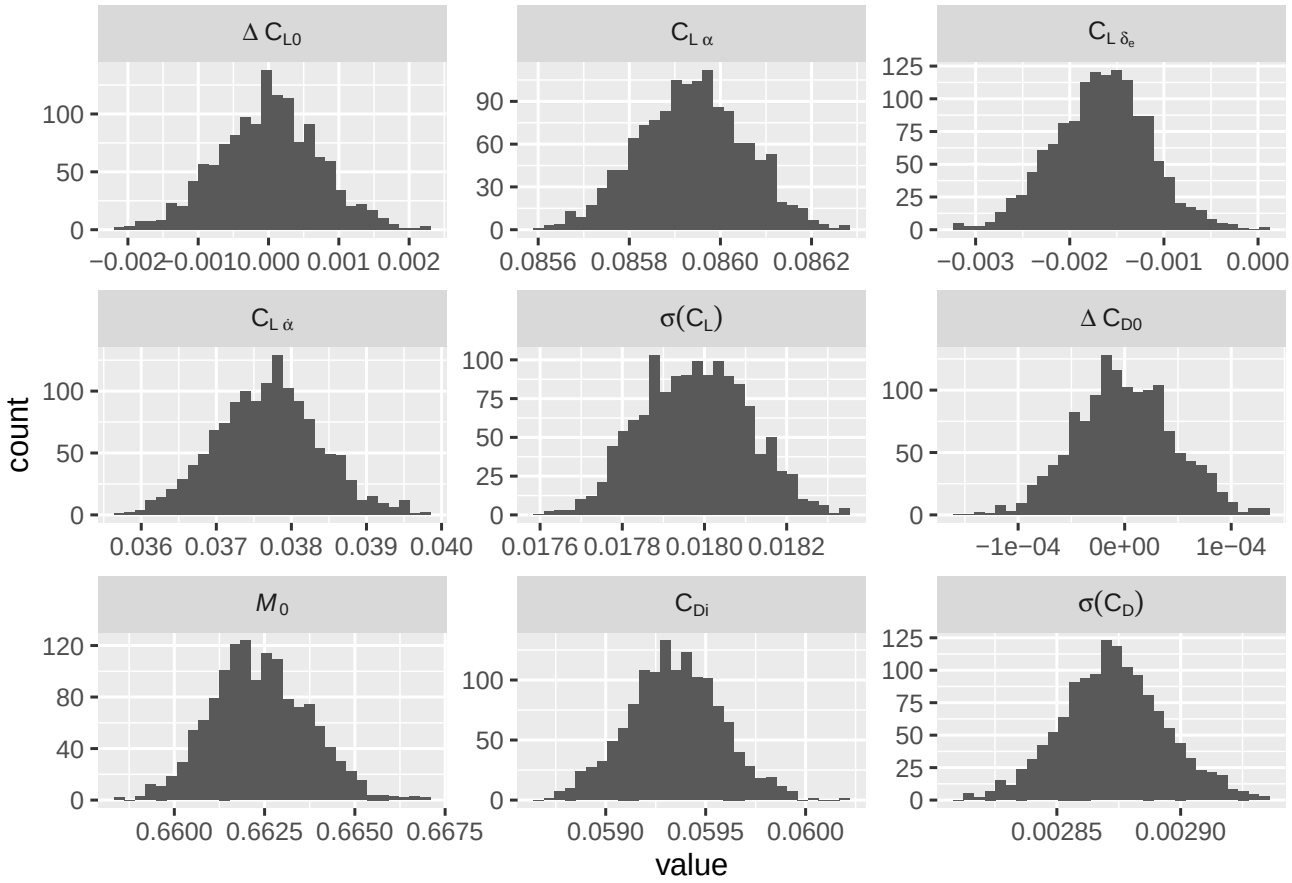

Figure 5 – Histograms of estimated parameters

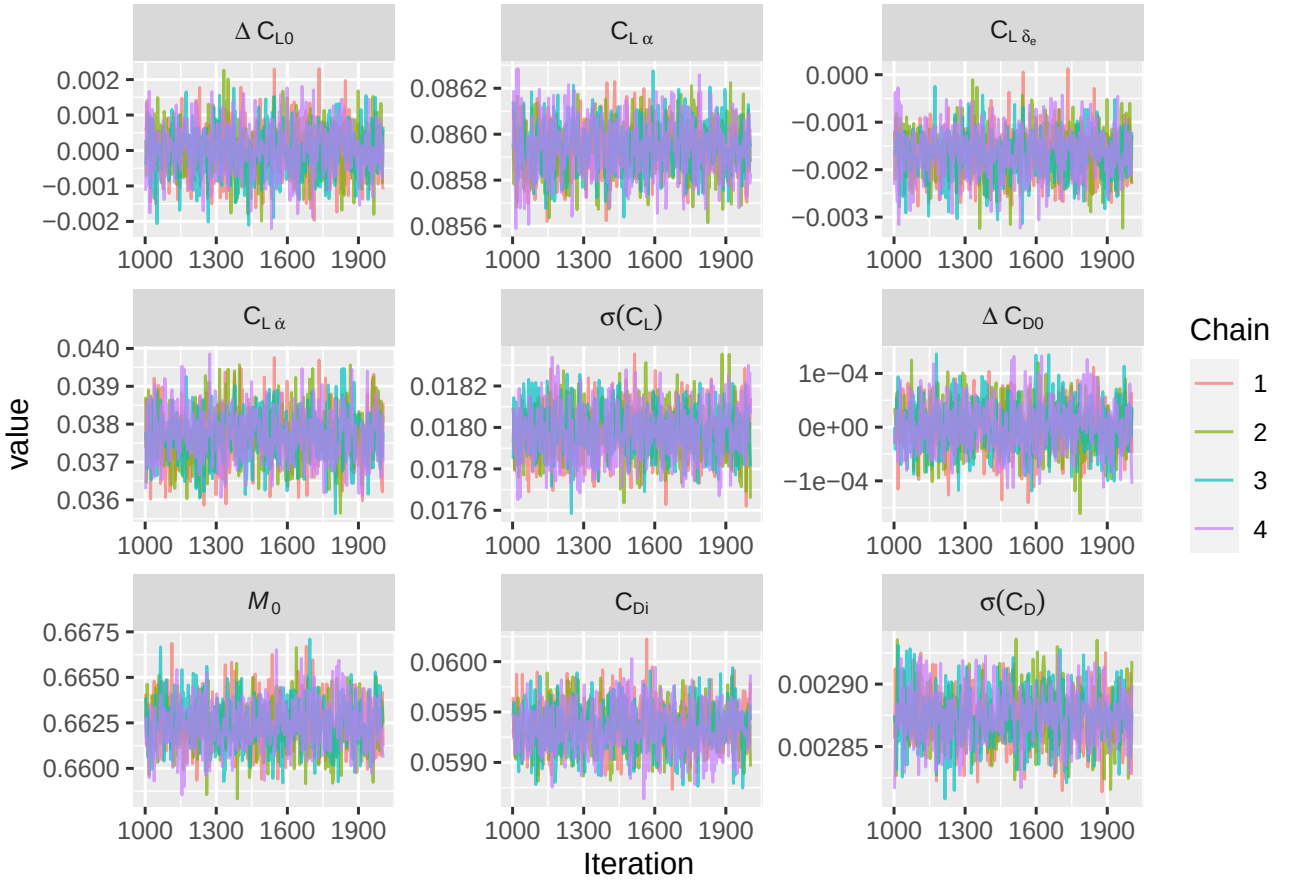

Figure 6 – Trace plots of estimated parameters

The main evaluations were performed with the plots of the lift slope and drag polar shown in Figs. 7 and 8. The observed samples, that is, the input flight data, are represented by the small circles. The shallow and dense blue areas are the 95% and 50% prediction intervals, respectively. These intervals were calculated with the generated random samples of the estimated parameters. Although only the variation of the angle of attack was taken into account, most of the observed samples, which were affected by the other factors, are located in or near the blue areas. This additionally proves that the estimated model approximated the actual flight data.

3.2 Necessity to consider the dynamic components

By comparing the three combinations of the datasets and the models, the fact that the best results were obtained with the large dataset and the model inclusion of the dynamic components will be clarified. As the metric of the goodness of the estimation results, the standard deviations of the estimated parameters were selected. Table 2 shows the estimation results of the three combinations: the small dataset without the model inclusion of the dynamic components, and the large dataset with and without the model inclusion. The standard deviations of the large dataset with the $C_{L\dot{\alpha}}$ consideration are lower than those of the other two combinations. Among the parameters, ΔC_{L0} was significantly improved with the model inclusion as shown in Fig. 9. Therefore, it is concluded that the best estimation was the large dataset with the model inclusion of the $C_{L\dot{\alpha}}$ components.

This fact means that it is natural but important to use an appropriate postulation for a model according to an input dataset. In addition, we have to pay much attention even if a mismatch between dataset and model is small. Figure 10, which is the scatter plot of the small and large datasets, shows the mismatch of the lift estimation. The horizontal and vertical axes correspond to the angular speeds q and the difference between the observations and the model outputs without the dynamic components, respectively. The model outputs are calculated with the estimated sample means, which are indicated with an over line like $\overline{C_{L0}}$ in the figure. Most of the points of the small and large datasets are located in the small area around the origin, that means they are in the good agreement with the model without the dynamic components. However, the other small number points of the large dataset are not.

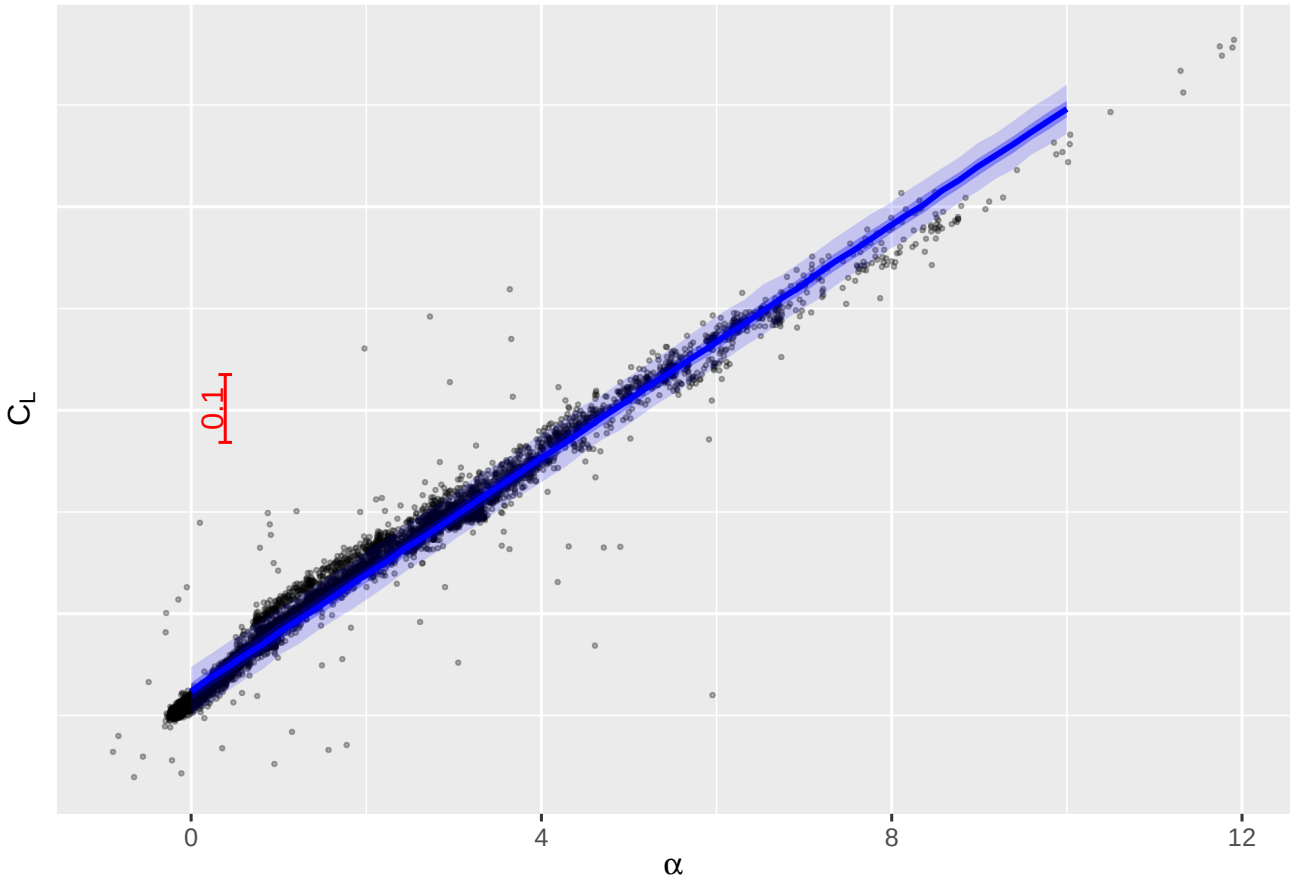

Figure 7 – Lift slope

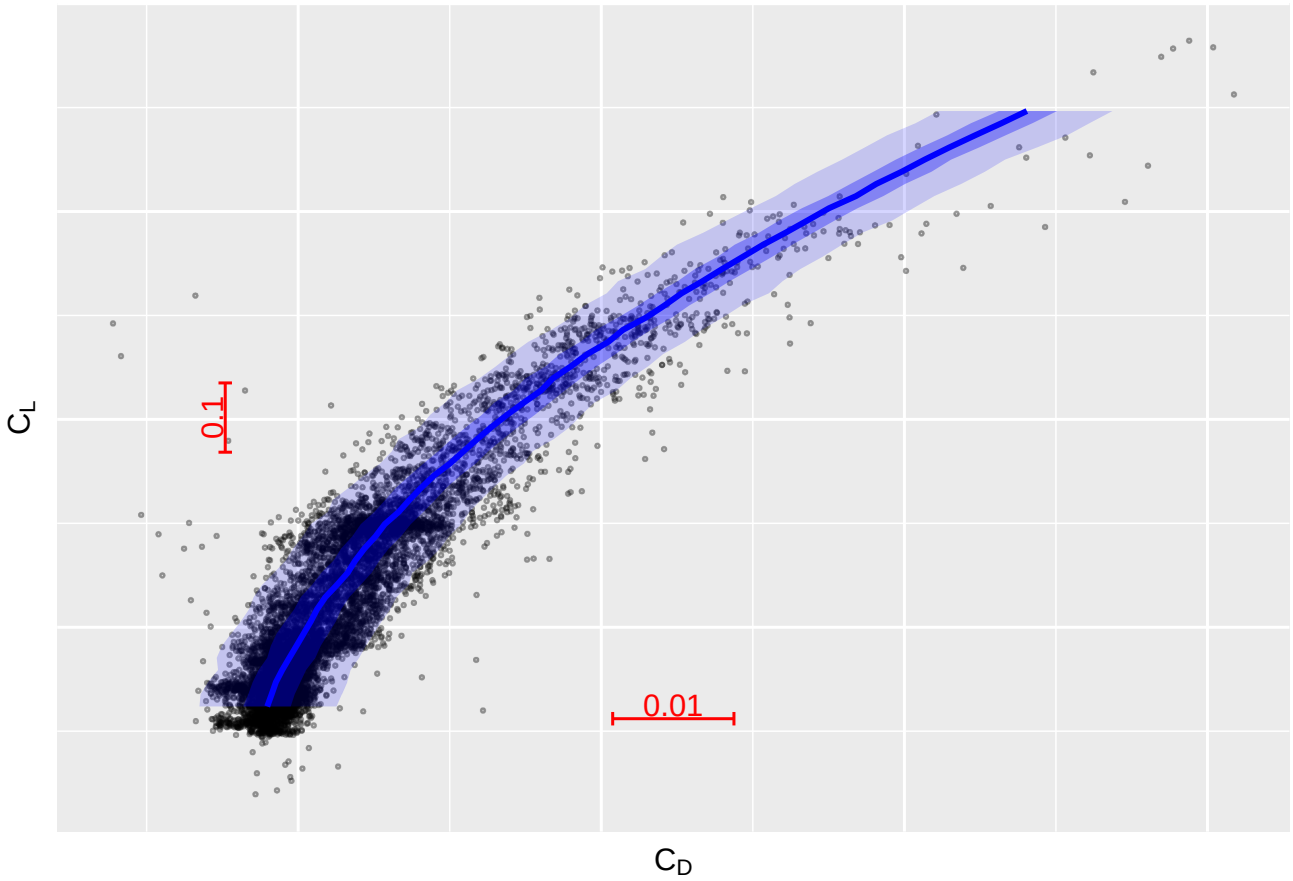

Figure 8 – Drag polar

Table 2 – Estimation results of three different combinations of datasets and models

Item	Small dataset (w/o $C_{L\dot{\alpha}}$)		Large dataset w/o $C_{L\dot{\alpha}}$		Large dataset with $C_{L\dot{\alpha}}$	
	Mean	Standard deviation	Mean	Standard deviation	Mean	Standard deviation
ΔC_{L0}	(0.000)	8.160×10^{-4}	(0.000)	7.964×10^{-4}	(0.000)	7.187×10^{-4}
$C_{L\alpha}$ [*1]	8.576×10^{-2}	1.194×10^{-4}	8.495×10^{-2}	1.325×10^{-4}	8.594×10^{-2}	1.166×10^{-4}
$C_{L\delta_e}$	-5.170×10^{-3}	5.516×10^{-4}	-1.145×10^{-2}	5.480×10^{-4}	-1.663×10^{-3}	5.070×10^{-4}
$C_{L\dot{\alpha}}$ [*2]	—	—	—	—	3.768×10^{-2}	6.932×10^{-4}
$\sigma(C_L)$	1.762×10^{-2}	1.422×10^{-4}	2.075×10^{-2}	1.530×10^{-4}	1.798×10^{-2}	1.292×10^{-4}

[*1] $[1/\mathrm{deg}]$ [*2] $[1/(\mathrm{deg/s})]$

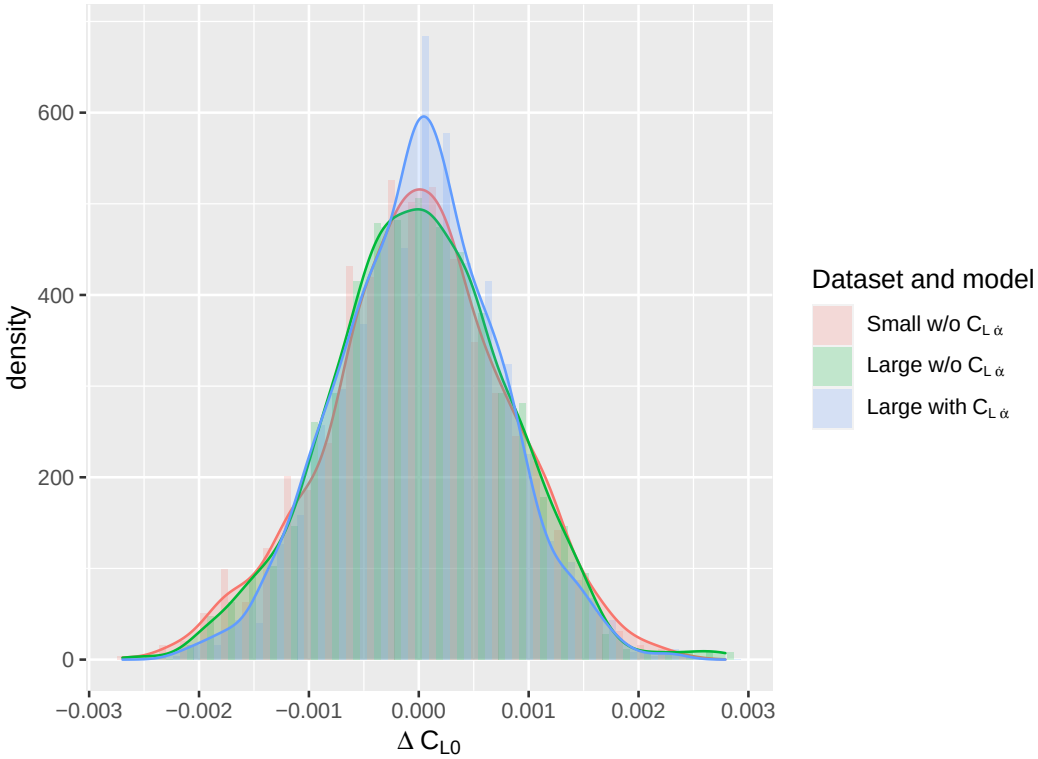

Figure 9 – Distribution of ΔC_{L0} estimations

Therefore, such small difference consequently required the additional consideration of the dynamic components for the large dataset. It is also proven with the regression lines $C_{L\dot{\alpha}q}$ estimated with the best combination. The lines are shown in blue color in the figure, and they well approximated the points located far from the origin.

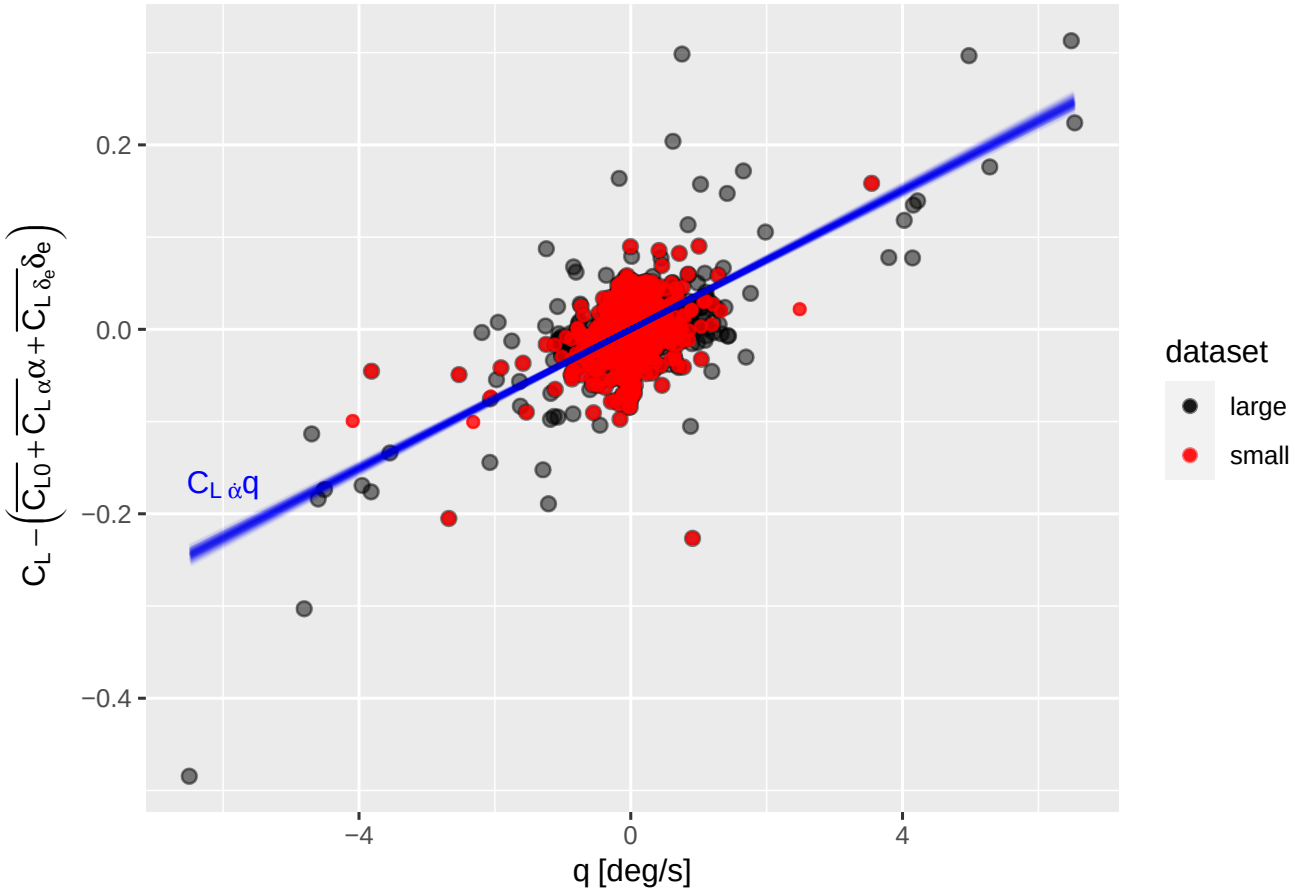

Figure 10 – Angular speed q and its C_L contribution

3.3 Wave drag estimation

In addition to the discussion of the dynamic component of the lift modeling, the estimation of the wave drag has a discussion. Figure 11 shows the scatter plot, which shows the relationship between Mach number M and the estimated wave drag components. As same as Fig. 9, the vertical position of the observed samples are calculated by using the sample means of the estimated parameters. The estimated wave drag model is displayed with the blue lines. In addition, the estimated drag divergent Mach numbers M_{DD}, in which a drag rise by 20 drag counts, i.e., 0.0020 C_D, occurs, are indicated with the vertical red lines. The estimated M_{DD} is qualitatively reasonable because it is located near the starting Mach number 0.8 of the typical transonic region.

However, whether the estimation is successful or not has still been questionable, because this may result from the postulated equation. In other words, if we use another approximated function, for example, a polynomial having a different exponential order, we may get another result. Therefore, to compare with other results of wind tunnel tests and CFD analyses will be planned in the future study.

4. Conclusion

This study demonstrated the modeling of the lift and drag aerodynamic force worked on the fixed-wing aircraft. It was performed with the MCMC sampling technique in the Bayesian inference framework. The comprehensive information about the modeling, that is, the postulated model, input flight data, and Stan of the MCMC sampler, were provided. The proposal to consider both the static and dynamic components was effective, which was confirmed by the comparison of the combination of the datasets and models. To say other general words, the fact that a small difference between a dataset and a

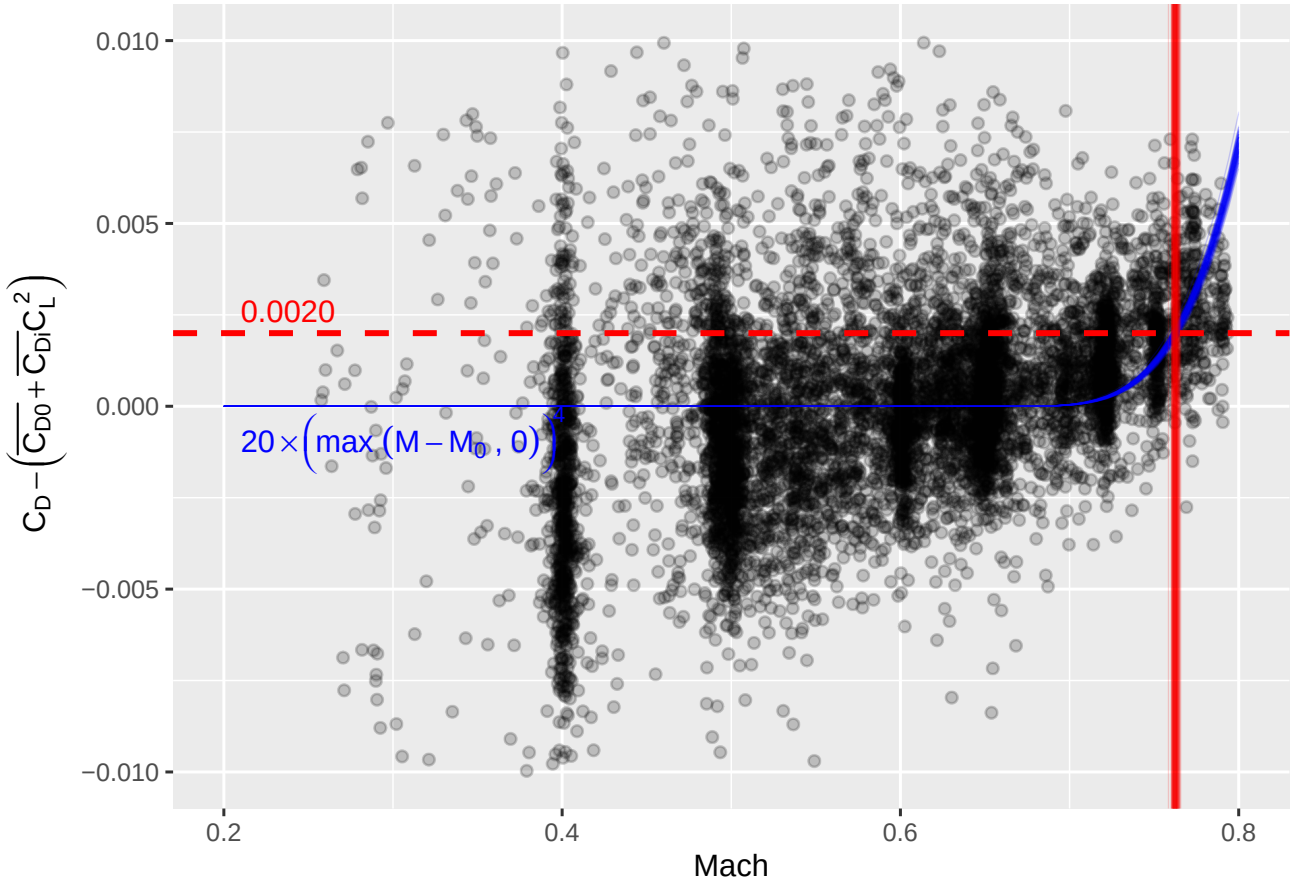

Figure 11 – Wave drag estimation

postulated model affects estimation results was acquired. Therefore, iterative update the postulation of the model based on the experimental, analytical, and empirical knowledge is the future work of this study.

Acknowledgment

This work was supported by JSPS KAKENHI Grant JP21381031.

Contact Author Email Address

naruoka.masaru@jaxa.jp

Copyright Statement

References

[1] A. Nuic. User manual for the base of aircraft data (bada) 3.12. Technical report, EUROCONTROL, 2014.

[2] Junzi Sun, Jacco M Hoekstra, and Joost Ellerbroek. Aircraft drag polar estimation based on a stochastic hierarchical model. In *8th International Conference on Research in Air Transportation*, 12 2018.

[3] Ravindra V. Jategaonkar. *Flight Vehicle System Identification: A Time-Domain Methodology, Second Edition*. American Institute of Aeronautics and Astronautics, Inc., January 2015.

[4] Eugene A. Morelli and Vladislav Klein. *Aircraft System Identification: Theory and Practice*. AIAA, 2006.

[5] M. Naruoka. Bayesian approach to flight characteristics modeling with real flight data. In *ICAS2018, 31th International Congress of the Aeronautical Sciences, Belo Horizonte, Brazil*, Sep 2018.

[6] Christopher M. Bishop. *Pattern Recognition and Machine Learning*. Springer, 2006.

[7] Bob Carpenter, Daniel Lee, Marcus A. Brubaker, Allen Riddell, Andrew Gelman, Ben Goodrich, Jiqiang Guo, Matt Hoffman, Michael Betancourt, and Peter Li. Stan: A probabilistic programming language, 2017.

[8] D.P. Raymer. *Aircraft Design: A Conceptual Approach*. AIAA education series. American Institute of Aeronautics and Astronautics, 2012.

[9] Antonio Filippone. Comprehensive analysis of transport aircraft flight performance. *Progress in Aerospace Sciences*, Vol. 44, No. 3, pp. 192–236, Apr 2008.

[10] H. Tomita, K. Masui, K. Hozumi, M. Naruoka, A. Yokoyama, S. Sumii, S. Ito, T. Oshima, and N. Tanaka. A Network-Based Flight Data Acquisition System of the JAXA Flying Test Bed "Hisho". In *Proceedings of the 50th Aircraft Symposium*, pp. 2819–2827, Nov. 2012. 2B07 (in Japanese).

[11] Andrew Gelman, John B Carlin, Hal S Stern, and Donald B Rubin. *Bayesian data analysis*. Chapman and Hall/CRC, 1995.